ISSN 0915-633X

NATIONAL INSTITUTE FOR FUSION SCIENCE

High Ion Temperature Mode in CHS Heliotron/torsatron Plasmas

K. Ida, S. Nishimura, T. Minami, K. Tanaka, S. Okamura,
M. Osakabe, H. Idei, S. Kubo, C. Takahashi and K. Matsuoka

(Received - Nov. 28, 1997)

NIFS-521 Nov. 1997

RESEARCH REPORT
NIFS Series

NAGOYA, JAPAN

High ion temperature mode in CHS Heliotron/torsatron plasmas

K.Ida, S.Nishimura, T.Minami, K.Tanaka, S.Okamura, M.Osakabe, H.Idei, S.Kubo, C.Takahashi, K.Matsuoka

National Institute for Fusion Science

Oroshi-cho, Toki-shi, Gifu, 509-52, Japan

Abstract

High ion temperature mode (high T_i mode) is observed for neutral beam heated plasmas in Compact Helical System (CHS) Heliotron/torsatron plasmas. The high T_i mode plasma is characterized by a peaked ion temperature profile and is associated with a peaked electron density profile produced by neutral beam fueling. The reduction of ion thermal diffusivity is observed at the plasma core ($\rho = 0.1$) in the high T_i mode by a factor of two. The high $T_i$mode discharge is observed only in the low density and the upper limit of n_e (critical n_e) for the high T_i mode depends on the density peaking factor.

keywords

High T_i mode, Compact Helical System, Improved mode, Density peaking, Radial electric field, Charge-exchange spectroscopy

1 Introduction

The high ion temperature (T_i) mode plasma is one of the improved modes in in Heliotron/torsatron and in stellarator[1]. It has many similar characteristics to that observed in super shots in TFTR [2], hot ion modes in JET and in JT-60 [3,4]. The high T_i mode is characterized by a high central ion temperature and low central ion thermal diffusivity, associated with a peaked electron density profile produced by neutral beam (NB) fueling with low wall recycling. Recently, similar high T_i mode discharges have been observed for neutral beam heated plasmas by turning off the gas puff at the onset of neutral beam in Heliotron-E devices[5,6]. Characteristics and operation regime of the high T_i mode discharges in CHS are studied. The electron density and its profiles are measured with scanning 3 chord FIR interferometer, 24 points, YAG thomson scattering, while the ion temperature and its profiles are measured with 30 points charges exchange spectroscopy (CXS) using fully stripped carbon[7]. The radial electric field profiles are derived from poloidal rotation velocity profile and carbon pressure profile measured with CXS.

2 Characteristics of high T_i mode discharges

Figure 1 shows the time evolution of central electron density, density peaking factor, $n_e(0)/\langle n_e \rangle$, where $\langle\rangle$ denotes volume average, central ion and electron temperature for the discharges without gas puff (high T_i mode) and with gas puff (L mode). The target plasma is produced by electron cyclotron resonance heating (ECH) pulse produces a target plasma for 14-40ms and neutral beam is injected for 40-140ms with the energy of 37keV, the beam current of 46A, the injected power of 900kW. The NB is tangentially injected to the plasma, where the magnetic axis of plasma is 92.1cm and the tangential radius of NB is 87cm. The helical magnetic field is 1.76T. When the electron density increases in time with gas puffing (t = 20 - 100 ms), the ion temperature stays almost constant in time (~ 0.4 keV) in the L-mode discharges. However, when the gas puff is turned off at t = 40 ms after the neutral beam injection, both central electron density, $n_e(0)$, and central ion temperature, $T_i(0)$, increase in time and the central ion temperature reaches 0.7 keV at t = 70 ms then decreases to the L mode levels (0.4keV) as the electron density is increased. The transition between

the high T_i mode and L mode is sensitive to the fraction of beam fueling to the gas puff fueling and a small amount gas puff or high wall recycling due to insufficient Titanium flash will prevent the discharge get into the high T_i mode.

The absolute value of $n_e(0)$ in the high T_i mode is similar to that in the early phase of L mode discharge. For example, $n_e(0)$ at t = 70ms in the L mode discharge is almost identical to the $n_e(0)$ at t = 90ms in the high T_i mode discharge. On the other hand, clear differences in the n_e profiles are observed between the high T_i mode discharge and L mode discharges. In the high T_i mode discharge, the electron density profile is peaked (~ 1.5), while it is flat (~ 1.0) in the L mode during gas puff (t < 100ms). Although the electron density profiles in the L mode also become peaked after the gas puff is turned off, the electron density seems to be too high for the transition to the high T_i mode late in the discharges. One of the characteristic of high T_i mode is ion temperature is higher than the electron temperature, although the two third of the neutral beam power deposits to electrons. The transport analysis has been done for the time sliced data at t = 90ms for the high T_i mode discharge and for the L mode discharge. The reduction of ion thermal diffusivity, χ_i , in the high T_i mode compared with that in L mode is a factor of two at the plasma core of $\rho < 0.8$, while the electron thermal diffusivity, χ_e, in the high T_i mode is even higher than that in L mode.

Figure 2 shows electron density, temperature, ion temperature and radial electric field for one high T_i mode discharge and for three L mode discharges with various gas puff rate. In the L mode discharges, ion temperature has weak dependence on electron density as $T_i(0) \propto n_e(0)^{-0.67}$. However, at the boundary between the the high T_i mode and L mode, even small increase of electron density, $\Delta n_e(0) = 15\%$, results in the large drop of ion temperature by 30% and plasma shows transition to the L mode. Clear differences between in the high T_i mode discharge and three L mode discharges are also observed in the electron temperature and radial electric field profiles. The tiny change in T_e profiles in L mode is due to the fact that increase of n_e is compensated by the increase of NB deposition power in the low density region. In the high T_i mode, the radial electric field is more negative and radial electric field shear is also larger than those in L mode. These characteristics suggest the hypothesis that radial electric field and shear improve ion transport but not electron transport.

At the low density region, the fraction of beam deposition power to the injected power

strongly depends on the electron density, and temperature shows no dependence on electron density as seen in Fig.2(b). In order to study the difference of density dependence of the ion and electron temperature, the central plasma ion and electron pressure are plotted as a function of central electron density for the constant injected power in Fig.3. The electron pressure shows linear density dependence at the low density $n_e(0) < 2.0 \times 10^{19} m^{-3}$, which is partly due to the change of deposition power of neutral beam, while the electron pressure shows saturation for higher density of $n_e(0) > 2.0 \times 10^{19} m^{-3}$. On the other hand, the ion pressure shows linear density dependence even at the higher density. Fig3(b) also shows the density regime for the high T_i mode discharge for this discharge is $1.5 - 2.5 \times 10^{19} m^{-3}$, where the ion pressure is higher but the electron pressure is even lower than that in L mode discharges. These data show that the ion confinement is improved but the electron confinement is degradated in the high T_i mode.

3 Operation regime of high T_i mode discharges

Fig.4(a) shows ion temperature as a function of central electron density for various gas puff at t = 70, 90, 110ms. At the low density regime (t = 70 and 90 ms), there are sharp change of $T_i(0)$ at $n_e(0) = 1.4 \times 10^{19} m^{-3}$ (t = 70ms) and $n_e(0) = 2.2 \times 10^{19} m^{-3}$ (t = 90ms) , which indicates the transition from L mode to high T_i mode. The density peaking factor in the high T_i mode are 1.5 (t = 70ms) and 1.8 (t = 90ms). However, there is no sharp change (transition to the high T_i mode discharge) observed at t = 110ms because the electron density exceeds the upper limit for the high T_i mode. The high T_i mode is observed at only low density plasma and the upper limit of the electron density for the high T_i mode increases as the peaking factor of electron density is increased. The dependence of critical ne(0) on the peaking factor is more clearly seen in Fig.4(b) which shows operation regime of high T_i mode discharges. T_i at the boundary between the high T_i mode and L mode is roughly 0.5 keV as seen in Fig4(a). The discharge with the ion temperature higher than 0.5 keV (high T_i mode plasma) are restricted in the lower $n_e(0)$ and higher ne(0)/<ne>.

There is a minimum $n_e(0)$ for the high T_i mode discharges. This is mainly due to the lack of enough beam deposition and fueling at the very low density. The transition from L mode to high T_i mode is observed in the range of central electron density of $1 \times 10^{19} m^{-3}$ to $3 \times 10^{19} m^{-3}$ and the

upper limit of the volume averaged electron density increases as the central electron density is increased.

When the recycling is high due to the poor wall condition, the central electron density increases without gas puff but the density peaking factor is low (< 1) then the plasma is always in the L mode. To achieve high T_i mode discharge, the peaking factor should increase as the central electron density increases. Therefore the central fueling by neutral beam is key for the high T_i mode. The high T_i mode due to pellet injection[8] observed in Heliotron-E also suggests that central fueling is important for the high T_i mode. The upper limit of electron density should depend on neutral beam heating power, magnetic field as well as peaking factor. Since the high T_i mode is observed only in the high field of >1.7T and with high power NBI > 0.8MW with low recycling wall condition in CHS, the dependence of the upper limit on heating power and magnetic field is not clear yet.

References

[1] A.Iiyoshi, in Fusion Energy (Porc. 16th Int. Conf. on Fusion energy, Montreal, 1996) IAEA Vienna Vol.1, (1997) 113..

[2] R.J.Fonck, et al., Phys. Rev. Lett. **63**, (1989) 520 .

[3] H.Weisen et al., Nucl. Fusion **29**, (1989) 2187 .

[4] Y.Koide, et al., Nucl. Fusion **33**, (1993) 251.

[5] K.Ida, et al., Phys. Rev. Lett. **76** (1996) 1268.

[6] K.Ida, et al., in Fusion Energy (Proc. 16th Int. Conf. on Fusion Energy, Montreal, 1996) IAEA Vienna Vol.2 (1997).

[7] K.Ida, S.Hidekuma, Rev. Sci. Instrum. **60**, (1989) 867.

[8] K.Ida, et al., Plasma Phys. 38 (1996) 1433.

Figure Captions

Fig.1 Time evolution of (a) central ion and electron temperature, (b) central electron density and its peaking factor $n_e(0)/\langle n_e \rangle$ and (c) the central ion and electron temperature as a function of central electron density (d) radial profiles of the ratio of ion and electron thermal diffusivity in high T_i mode to that in L-mode discharges. The arrows in Fig.(c) stand for the time sliced data used in the transport analysis for χ_i and χ_e profiles in Fig.(d).

Fig.2 Radial profiles of (a) electron density, (b) electron temperature, (c) ion temperature, and (d) radial electric field for various rate of gas puffing (one is high T_i mode discharge and three are L-mode discharges).

Fig.3 Central (a) electron and (b) ion pressure as a function of central electron density for various rate of gas puffing (one is high T_i mode discharge and three are L-mode discharges).

Fig.4 (a) Central ion temperature as a function of central electron density and (b) operation regime of high T_i mode discharges. The values of peaking factor $n_e(0)\langle n_e \rangle$ are also plotted in Fig.4(a).

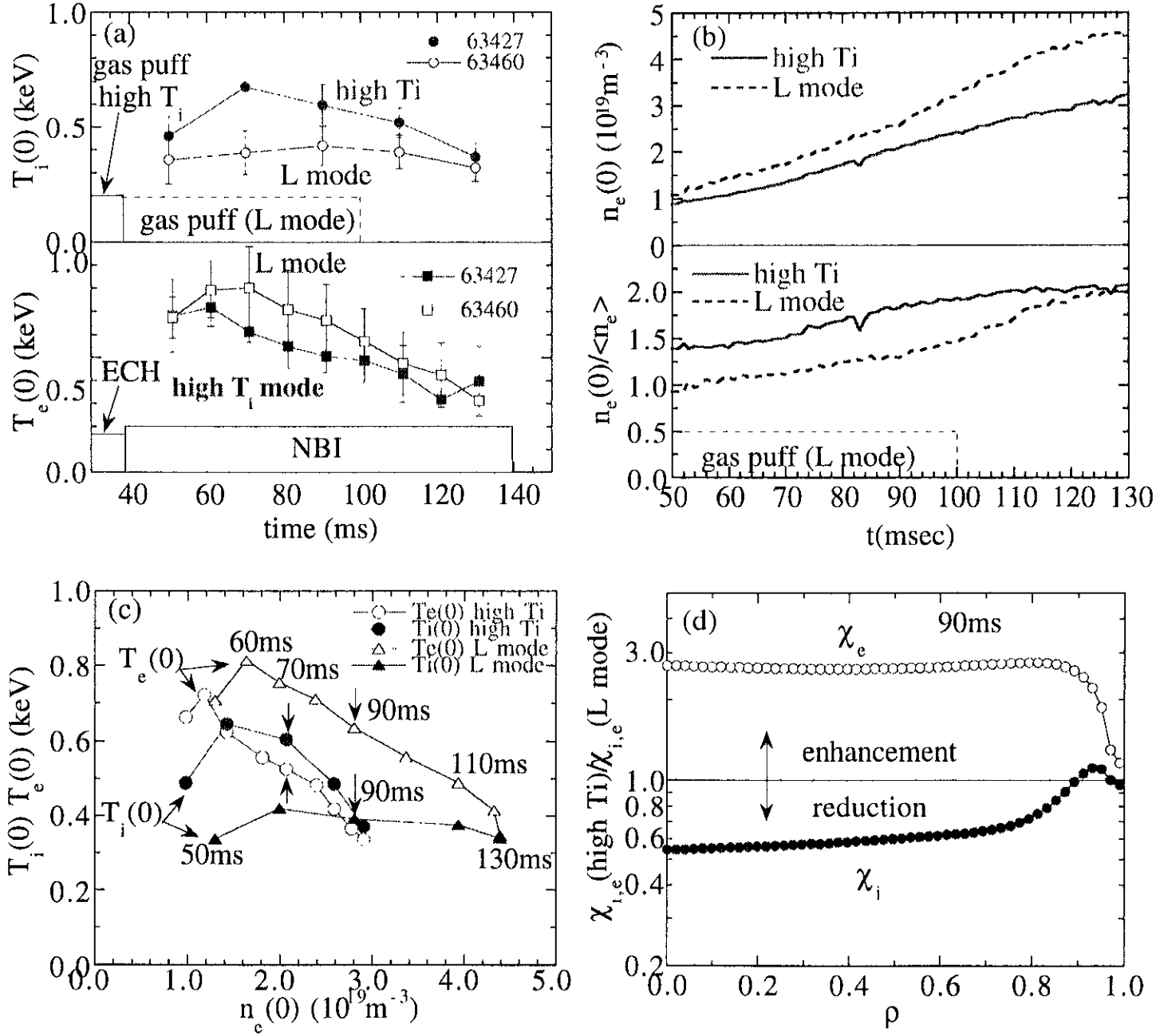
(a)
63427
63460
gas puff
high T_i
high Ti
L mode
gas puff (L mode)
$T_i(0)$ (keV)
L mode
63427
63460
ECH
high T_i mode
NBI
$T_e(0)$ (keV)
time (ms)
(b)
high Ti
L mode
$n_e(0)$ ($10^{19}m^{-3}$)
high Ti
L mode
$n_e(0)/<n_e>$
gas puff (L mode)
t(msec)
(c)
Te(0) high Ti
Ti(0) high Ti
Te(0) L mode
Ti(0) L mode
$T_e(0)$
60ms
70ms
90ms
110ms
$T_i(0)$
90ms
50ms
130ms
$T_i(0)$ $T_e(0)$ (keV)
$n_e(0)$ ($10^{19}m^{-3}$)
(d)
χ_e
90ms
enhancement
reduction
χ_i
$\chi_{i,e}$ (high Ti)/$\chi_{i,e}$ (L mode)
ρ

Fig.1

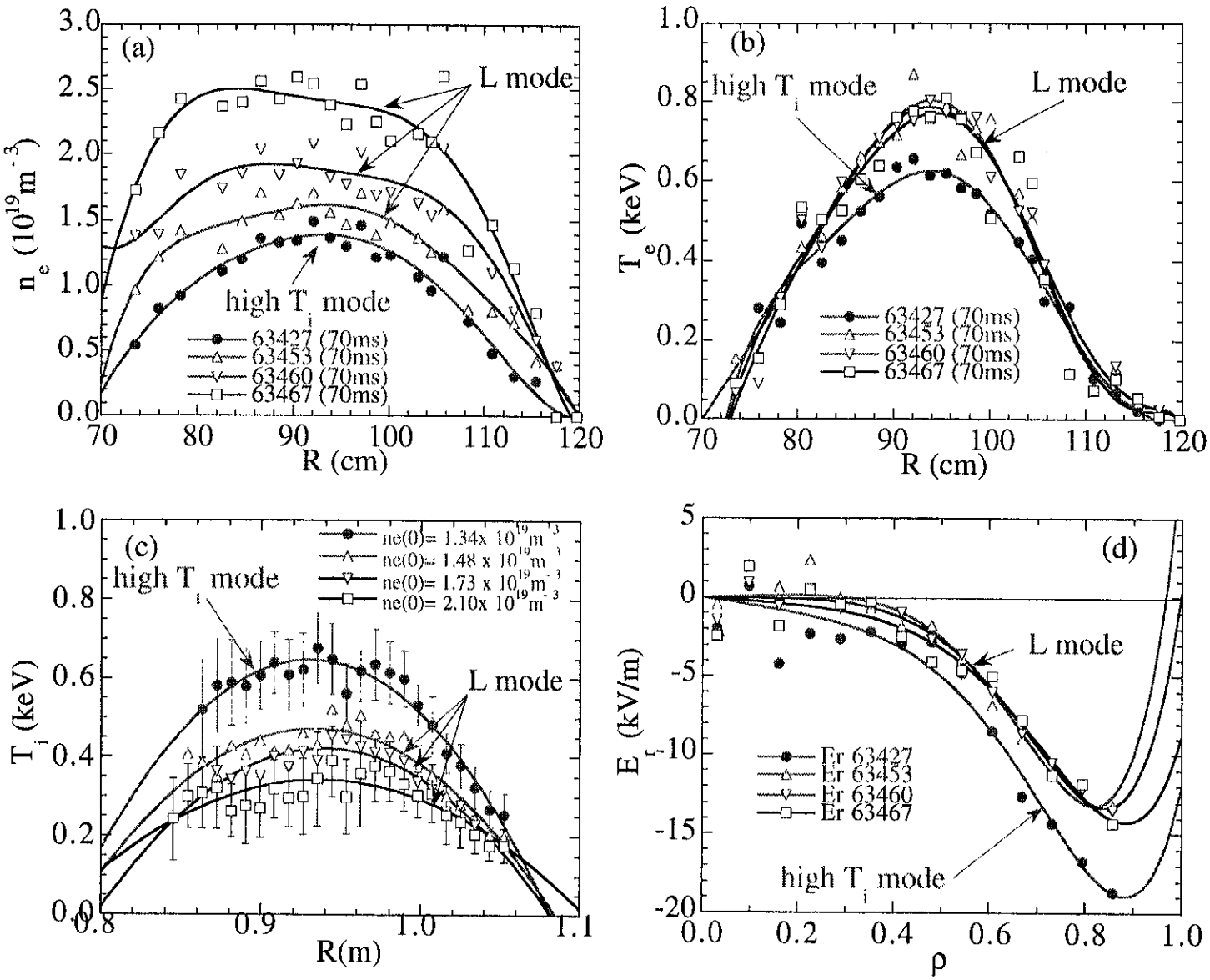
(a)
L mode
high T_i mode
63427 (70ms)
63453 (70ms)
63460 (70ms)
63467 (70ms)
n_e (10^19 m^-3)
R (cm)
(b)
high T_i mode
L mode
T_e (keV)
R (cm)
(c)
high T_i mode
ne(0)= 1.34x 10^19 m^-3
ne(0)= 1.48 x 10^19 m^-3
ne(0)= 1.73 x 10^19 m^-3
ne(0)= 2.10x 10^19 m^-3
L mode
T_i (keV)
R(m)
(d)
L mode
Er 63427
Er 63453
Er 63460
Er 63467
high T_i mode
E_r (kV/m)
ρ

Fig.2

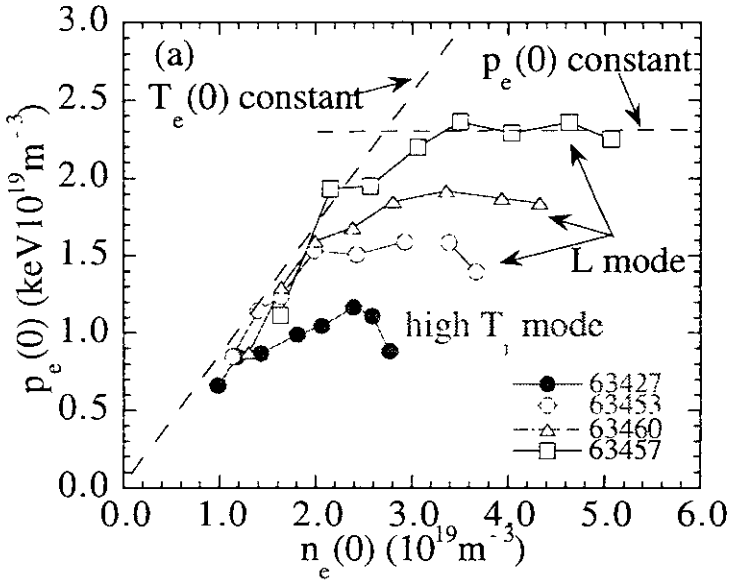
(a)
T_e(0) constant
p_e(0) constant
L mode
high T_i mode
63427
63453
63460
63457
p_e(0) (keV10^{19}m^{-3})
n_e(0) (10^{19}m^{-3})
0.0
0.5
1.0
1.5
2.0
2.5
3.0
0.0
1.0
2.0
3.0
4.0
5.0
6.0

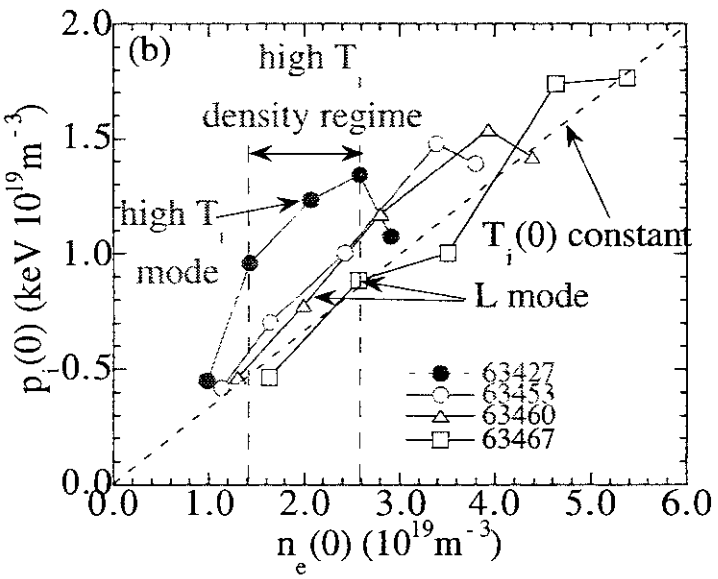
(b)
high T_i
density regime
high T_i
mode
T_i(0) constant
L mode
63427
63453
63460
63467
p_i(0) (keV 10^{19}m^{-3})
n_e(0) (10^{19}m^{-3})
0.0
0.5
1.0
1.5
2.0
0.0
1.0
2.0
3.0
4.0
5.0
6.0

Fig.3

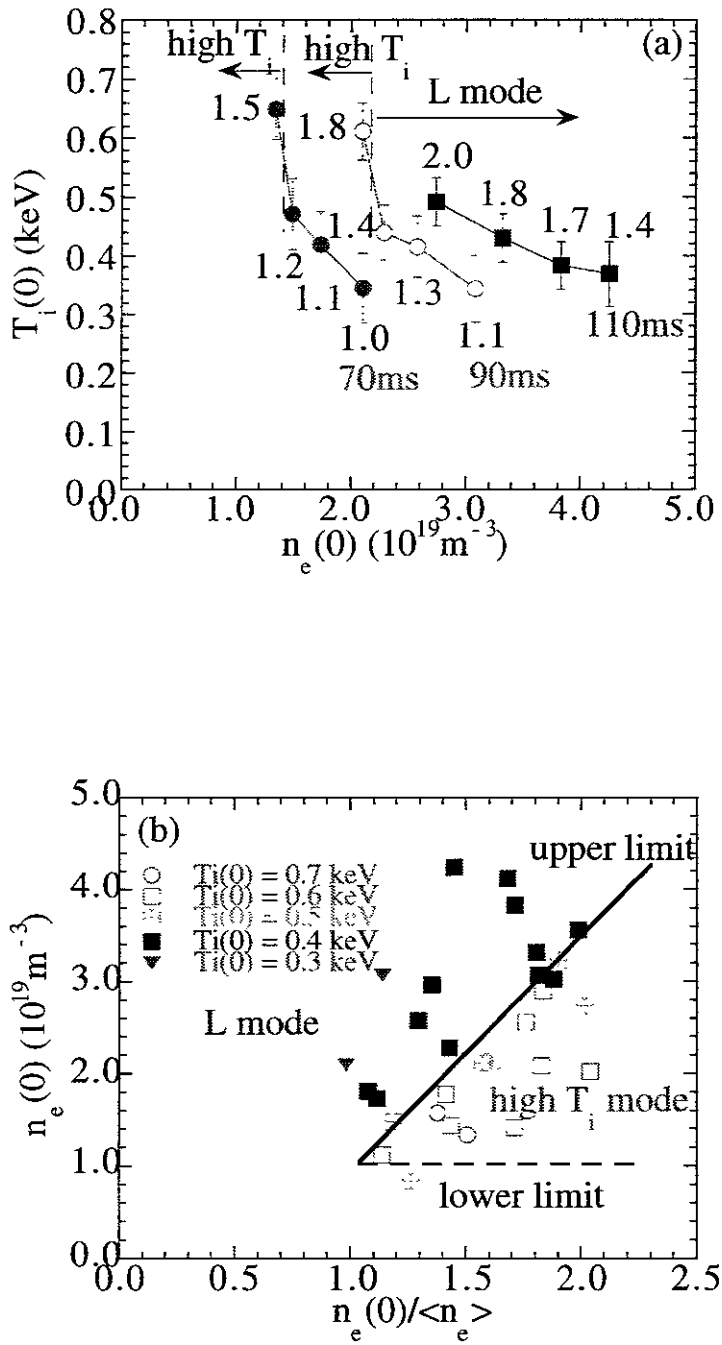
high T_i
high T_i
(a)
L mode
1.5
1.8
2.0
1.8
1.7
1.4
1.4
1.2
1.1
1.3
1.0
1.1
110ms
70ms
90ms
T_i(0) (keV)
n_e(0) (10^19 m^-3)
(b)
Ti(0) = 0.7 keV
Ti(0) = 0.6 keV
Ti(0) = 0.5 keV
Ti(0) = 0.4 keV
Ti(0) = 0.3 keV
upper limit
L mode
high T_i mode
lower limit
n_e(0) (10^19 m^-3)
n_e(0)/<n_e>

Fig.4

Recent Issues of NIFS Series

NIFS-473 S. Murakami, N. Nakajima, U. Gasparino and M. Okamoto,
Simulation Study of Radial Electric Field in CHS and LHD; Jan. 1997

NIFS-474 K. Ohkubo, S. Kubo, H. Idei, M. Sato, T. Shimozuma and Y. Takita,
Coupling of Tilting Gaussian Beam with Hybrid Mode in the Corrugated Waveguide; Jan. 1997

NIFS-475 A. Fujisawa, H. Iguchi, S. Lee and Y. Hamada,
Consideration of Fluctuation in Secondary Beam Intensity of Heavy Ion Beam Prove Measurements; Jan. 1997

NIFS-476 Y. Takeiri, M. Osakabe, Y. Oka, K. Tsumori, O. Kaneko, T. Takanashi, E. Asano, T. Kawamoto, R. Akiyama and T. Kuroda,
Long-pulse Operation of a Cesium-Seeded High-Current Large Negative Ion Source; Jan. 1997

NIFS-477 H. Kuramoto, K. Toi, N. Haraki, K. Sato, J. Xu, A. Ejiri, K. Narihara, T. Seki, S. Ohdachi, K. Adati, R. Akiyama, Y. Hamada, S. Hirokura, K. Kawahata and M. Kojima,
Study of Toroidal Current Penetration during Current Ramp in JIPP T-IIU with Fast Response Zeeman Polarimeter; Jan., 1997

NIFS-478 H. Sugama and W. Horton,
Neoclassical Electron and Ion Transport in Toroidally Rotating Plasmas; Jan. 1997

NIFS-479 V.L. Vdovin and I.V. Kamenskij,
3D Electromagnetic Theory of ICRF Multi Port Multi Loop Antenna; Jan. 1997

NIFS-480 W.X. Wang, M. Okamoto, N. Nakajima, S Murakami and N. Ohyabu,
Cooling Effect of Secondary Electrons in the High Temperature Divertor Operation; Feb. 1997

NIFS-481 K. Itoh, S.-I. Itoh, H. Soltwisch and H.R. Koslowski,
Generation of Toroidal Current Sheet at Sawtooth Crash; Feb. 1997

NIFS-482 K. Ichiguchi,
Collisionality Dependence of Mercier Stability in LHD Equilibria with Bootstrap Currents; Feb. 1997

NIFS-483 S. Fujiwara and T. Sato,
Molecular Dynamics Simulations of Structural Formation of a Single Polymer Chain: Bond-orientational Order and Conformational Defects; Feb. 1997

NIFS-484 T. Ohkawa,
Reduction of Turbulence by Sheared Toroidal Flow on a Flux Surface; Feb.

1997

NIFS-485 K. Narihara, K. Toi, Y. Hamada, K. Yamauchi, K. Adachi, I. Yamada, K. N. Sato, K. Kawahata, A. Nishizawa, S. Ohdachi, K. Sato, T. Seki, T. Watari, J. Xu, A. Ejiri, S. Hirokura, K. Ida, Y. Kawasumi, M. Kojima, H. Sakakita, T. Ido, K. Kitachi, J. Koog and H. Kuramoto,
Observation of Dusts by Laser Scattering Method in theJIPPT-IIU Tokamak Mar. 1997

NIFS-486 S. Bazdenkov, T. Sato and The Complexity Simulation Group,
Topological Transformations in Isolated Straight Magnetic Flux Tube; Mar. 1997

NIFS-487 M. Okamoto,
Configuration Studies of LHD Plasmas; Mar. 1997

NIFS-488 A. Fujisawa, H. Iguchi, H. Sanuki, K. Itoh, S. Lee, Y. Hamada, S. Kubo, H. Idei, R. Akiyama, K. Tanaka, T. Minami, K. Ida, S. Nishimura, S. Morita, M. Kojima, S. Hidekuma, S.-I. Itoh, C. Takahashi, N. Inoue, H. Suzuki, S. Okamura and K. Matsuoka,
Dynamic Behavior of Potential in the Plasma Core of the CHS Heliotron/Torsatron; Apr. 1997

NIFS-489 T. Ohkawa,
Pfirsch - Schlüter Diffusion with Anisotropic and Nonuniform Superthermal Ion Pressure; Apr. 1997

NIFS-490 S. Ishiguro and The Complexity Simulation Group,
Formation of Wave-front Pattern Accompanied by Current-driven Electrostatic Ion-cyclotron Instabilities; Apr. 1997

NIFS-491 A. Ejiri, K. Shinohara and K. Kawahata,
An Algorithm to Remove Fringe Jumps and its Application to Microwave Reflectometry; Apr. 1997

NIFS-492 K. Ichiguchi, N. Nakajima, M. Okamoto,
Bootstrap Current in the Large Helical Device with Unbalanced Helical Coil Currents; Apr. 1997

NIFS-493 S. Ishiguro, T. Sato, H. Takamaru and The Complexity Simulation Group,
V-shaped dc Potential Structure Caused by Current-driven Electrostatic Ion-cyclotron Instability; May 1997

NIFS-494 K. Nishimura, R. Horiuchi, T. Sato,
Tilt Stabilization by Energetic Ions Crossing Magnetic Separatrix in Field-Reversed Configuration; June 1997

NIFS-495 T. -H. Watanabe and T. Sato,
Magnetohydrodynamic Approach to the Feedback Instability; July 1997

NIFS-496 K. Itoh, T. Ohkawa, S. -I.Itoh, M. Yagi and A. Fukuyama

Suppression of Plasma Turbulence by Asymmetric Superthermal Ions; July 1997

NIFS-497 T. Takahashi, Y. Tomita, H. Momota and Nikita V. Shabrov,
Collisionless Pitch Angle Scattering of Plasma Ions at the Edge Region of an FRC; July 1997

NIFS-498 M. Tanaka, A.Yu Grosberg, V.S. Pande and T. Tanaka,
Molecular Dynamics and Structure Organization in Strongly-Coupled Chain of Charged Particles; July 1997

NIFS-499 S. Goto and S. Kida,
Direct-interaction Approximation and Reynolds-number Reversed Expansion for a Dynamical System; July 1997

NIFS-500 K. Tsuzuki, N. Inoue, A. Sagara, N. Noda, O. Motojima, T. Mochizuki, T. Hino and T. Yamashina,
Dynamic Behavior of Hydrogen Atoms with a Boronized Wall; July 1997

NIFS-501 I. Viniar and S. Sudo,
Multibarrel Repetitive Injector with a Porous Pellet Formation Unit; July 1997

NIFS-502 V. Vdovin, T. Watari and A. Fukuyama,
An Option of ICRF Ion Heating Scenario in Large Helical Device; July 1997

NIFS-503 E. Segre and S. Kida,
Late States of Incompressible 2D Decaying Vorticity Fields; Aug. 1997

NIFS-504 S. Fujiwara and T. Sato,
Molecular Dynamics Simulation of Structural Formation of Short Polymer Chains; Aug. 1997

NIFS-505 S. Bazdenkov and T. Sato
Low-Dimensional Model of Resistive Interchange Convection in Magnetized Plasmas; Sep. 1997

NIFS-506 H. Kitauchi and S. Kida,
Intensification of Magnetic Field by Concentrate-and-Stretch of Magnetic Flux Lines; Sep. 1997

NIFS-507 R.L. Dewar,
Reduced form of MHD Lagrangian for Ballooning Modes; Sep. 1997

NIFS-508 Y.-N. Nejoh,
Dynamics of the Dust Charging on Electrostatic Waves in a Dusty Plasma with Trapped Electrons; Sep.1997

NIFS-509 E. Matsunaga, T.Yabe and M. Tajima,

Baroclinic Vortex Generation by a Comet Shoemaker-Levy 9 Impact; Sep. 1997

NIFS-510 C.C. Hegna and N. Nakajima,
On the Stability of Mercier and Ballooning Modes in Stellarator Configurations; Oct. 1997

NIFS-511 K. Orito and T. Hatori,
Rotation and Oscillation of Nonlinear Dipole Vortex in the Drift-Unstable Plasma; Oct. 1997

NIFS-512 J. Uramoto,
Clear Detection of Negative Pionlike Particles from H_2 Gas Discharge in Magnetic Field; Oct. 1997

NIFS-513 T. Shimozuma, M. Sato, Y. Takita, S. Ito, S. Kubo, H. Idei, K. Ohkubo, T. Watari, T.S. Chu, K. Felch, P. Cahalan and C.M. Loring, Jr,
The First Preliminary Experiments on an 84 GHz Gyrotron with a Single-Stage Depressed Collector; Oct. 1997

NIFS-514 T. Shjmozuma, S. Morimoto, M. Sato, Y. Takita, S. Ito, S. Kubo, H. Idei, K. Ohkubo and T. Watari,
A Forced Gas-Cooled Single-Disk Window Using Silicon Nitride Composite for High Power CW Millimeter Waves; Oct. 1997

NIFS-515 K. Akaishi,
On the Solution of the Outgassing Equation for the Pump-down of an Unbaked Vacuum System; Oct. 1997

NIFS-516 *Papers Presented at the 6th H-mode Workshop (Seeon, Germany)*; Oct. 1997

NIFS-517 John L. Johnson,
The Quest for Fusion Energy; Oct. 1997

NIFS-518 J. Chen, N. Nakajima and M. Okamoto,
Shift-and-Inverse Lanczos Algorithm for Ideal MHD Stability Analysis; Nov. 1997

NIFS-519 M. Yokoyama, N. Nakajima and M. Okamoto,
Nonlinear Incompressible Poloidal Viscosity in L=2 Heliotron and Quasi-Symmetric Stellarators; Nov. 1997

NIFS-520 S. Kida and H. Miura,
Identificaiton and Analysis of Vortical Structures; Nov. 1997

NIFS-521 K. Ida, S. Nishimura, T. Minami, K. Tanaka, S. Okamura, M. Osakabe, H. Idei, S. Kubo, C. Takahashi and K. Matsuoka,
High Ion Temperature Mode in CHS Heliotron/torsatron Plasmas; Nov. 1997